Electronic Supplementary Material (ESI) for Journal of Materials Chemistry C.

ELECTRONIC SUPPLEMENTARY INFORMATION

Quantifying Local Thickness and Composition in Thin Films of Organic Photovoltaic Blends by Raman Scattering

Xabier Rodríguez-Martínez,*[1] Michelle S. Vezie,[2] Xingyuan Shi,[2] Iain McCulloch,[3,4] Jenny Nelson,[2] Alejandro R. Goñi[1,5] and Mariano Campoy-Quiles*[1]

* Corresponding authors. E-mail: xrodriguez@icmab.es, mcampoy@icmab.es
[1] Institut de Ciència de Materials de Barcelona (ICMAB-CSIC), Bellaterra, 08193, Spain
[2] Centre for Plastic Electronics and Department of Physics, Imperial College London, Prince Consort Road, London SW7 2AZ, UK
[3] Centre for Plastic Electronics and Department of Chemistry, Imperial College London, Exhibition Road, London SW7 2AZ, UK
[4] SPERC, King Abdullah University of Science and Technology, Thuwal 23955-6900, Saudi Arabia
[5] Institució Catalana de Recerca I Estudis Avançats (ICREA), Barcelona, 08010, Spain

ON THE APPLICATION OF THE METHODOLOGY IN A DIFFERENT RAMAN (BACKSCATTERING) SETUP

The general applicability of the Raman methodology presented in this work was double-checked in a second setup (Alpha300RA by WITec) employing the same geometry (backscattering) although different optics (50X magnification, NA = 0.8, or 10X magnification, NA = 0.25, both objectives manufactured by Zeiss) and CCD with respect to the LabRam setup used originally (20X magnification, NA = 0.35 by Olympus). As illustrated in Fig. S-1, the Raman intensity oscillation with film thickness in C16-IDTBT at 488 nm excitation was properly reproduced on the second setup regardless the objective employed.

Interestingly, the *effective* Raman cross-section (cts s^{-1} μW^{-1}) for this material was found to be nearly one order of magnitude lower in the second setup (WITec) as compared to the first one (LabRam) if the 10X magnification objective was used (see Table S-1); on the other hand, by selecting the 50X objective at the WITec setup the effective value obtained is comparable to that extracted at the original setup (LabRam) with lower magnification (20X). These trends demonstrate that the effective values of the Raman cross-sections may deviate significantly between different setups as a consequence of the different geometrical factors, including the numerical aperture, confocality and objective magnification as well as the CCD collection yield. Nevertheless, we double-checked that the Raman cross-section ratios between dissimilar materials were within the experimental error margin in both setups (see Table S-1), thus confirming the generality of the methodology.

We have also confirmed that the effective Raman cross-sections extracted for a given setup are independent of the type of substrate employed. As an example, C16-IDTBT showed a cross-section of $(3.1 \pm 0.6) \cdot 10^{-2}$ cts s^{-1} μW^{-1} when deposited on silicon, which is a value comparable to that obtained when the film was deposited on glass substrates $(3.0 \pm 0.3) \cdot 10^{-2}$ cts s^{-1} μW^{-1}) given the error committed on thickness and laser power determination. These results indicate that the distribution of the electric field in the multi-layered stack is properly modelled by the transfer matrix method.

Table S-1 List of effective solid-state Raman cross-sections for C16-IDTBT, PCBM and $PC_{70}BM$ at 488 nm excitation as extracted in two different setups with different geometrical factors and CCDs.

Raman setup	Material	Effective Raman cross-section (σ_R)	$\sigma_{R,u} / \sigma_{R,PC70BM}$
LabRam 20X, NA 0.35	C16-IDTBT	$(3.3 \pm 0.3) \cdot 10^{-2}$ cts s^{-1} μW^{-1}	8 ± 1
	PCBM	$(1.3 \pm 0.2) \cdot 10^{-3}$ cts s^{-1} μW^{-1}	0.3 ± 0.1
	$PC_{70}BM$	$(4.4 \pm 0.5) \cdot 10^{-3}$ cts s^{-1} μW^{-1}	1
WITec 50X, NA 0.80	C16-IDTBT	$(3.5 \pm 0.4) \cdot 10^{-2}$ cts s^{-1} μW^{-1}	8 ± 1
	PCBM	$(1.7 \pm 0.1) \cdot 10^{-3}$ cts s^{-1} μW^{-1}	0.41 ± 0.04
	$PC_{70}BM$	$(4.1 \pm 0.3) \cdot 10^{-3}$ cts s^{-1} μW^{-1}	1
WITec 10X, NA 0.25	C16-IDTBT	$(2.7 \pm 0.4) \cdot 10^{-3}$ cts s^{-1} μW^{-1}	-

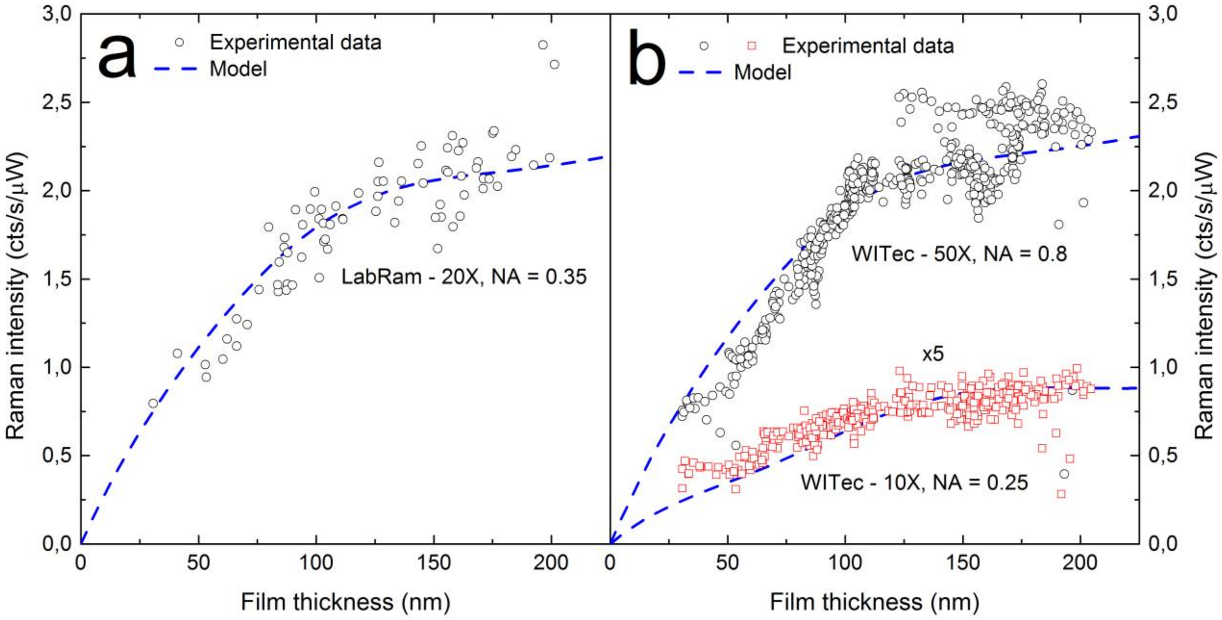

Figure S-1 Dependence of the 1353 cm^{-1} Raman band as a function of C16-IDTBT film thickness at 488 nm excitation as measured in two different setups: (a) LabRam HR800 (20X magnification, NA = 0.35) and (b) Alpha300RA by WITec (50X magnification, NA = 0.8, upper curve; and 10X magnification, NA = 0.25, lower curve with a five-fold magnification for better clarity).

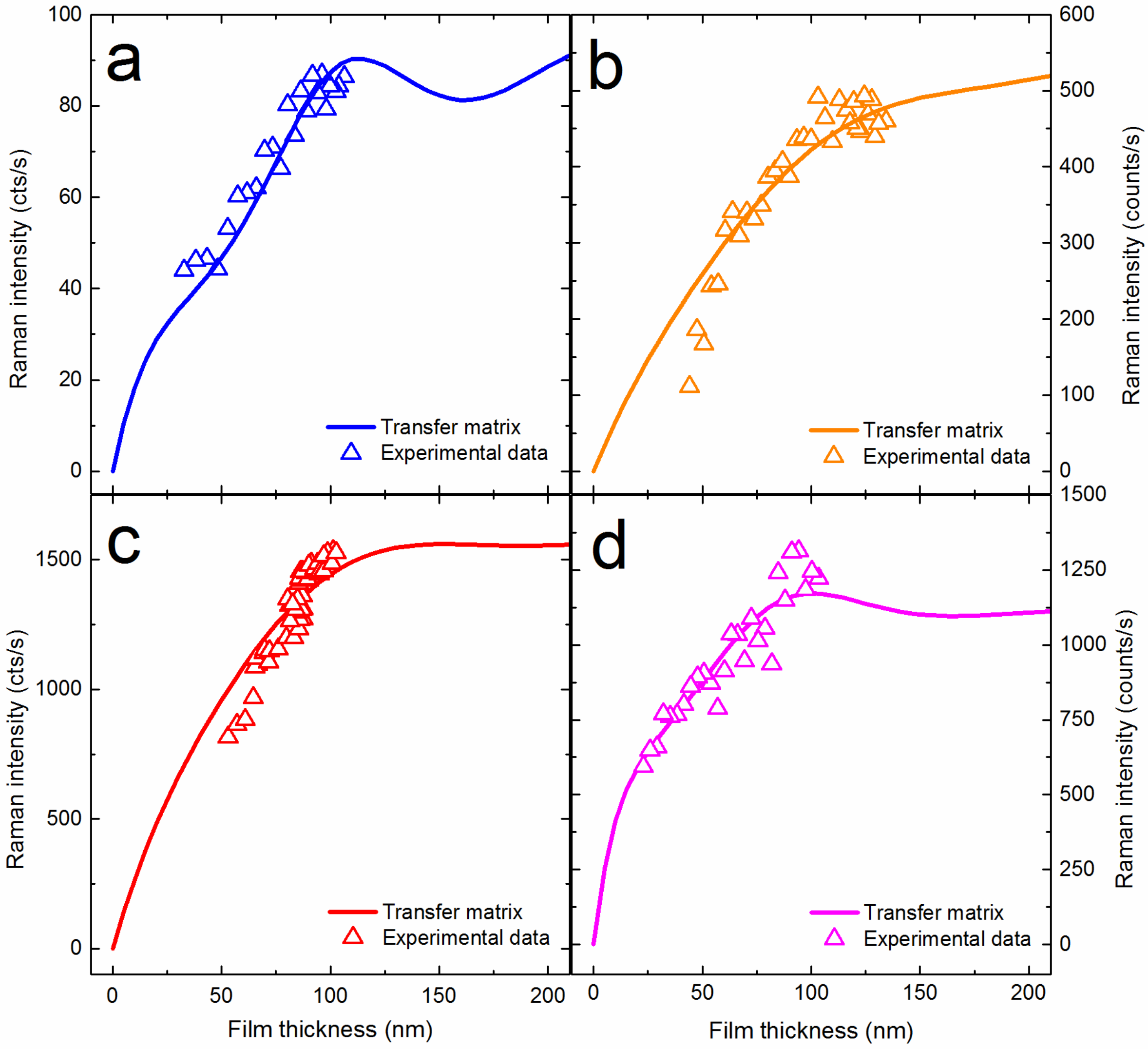

Figure S-2 Raman intensity (triangles) as a function of film thickness for (a) $PC_{70}BM$ at 488 nm excitation (1564 cm^{-1} band); (b) PCPDTBT at 488 nm excitation (1349 cm^{-1} band); (c) C16-IDTBT at 514 nm excitation (1353 cm^{-1} band); and (d) PCDTBT at 514 nm excitation (1445 cm^{-1} band). Solid lines stand for the transfer matrix modeling of the Raman process.

MULTI-WAVELENGTH FITTING APPROACH WITH SHARED PARAMETERS AS A WAY TO EXTEND THE SENSITIVITY OF THE METHODOLOGY REGARDING FILM THICKNESS DETERMINATION

The shape of the Raman interference curves is mainly determined by the optical constants at the excitation wavelength and at that shifted by the wavenumber of the mode under study. Resonant probing conditions usually lead to interference curves in which the first intensity maximum is reached for films below ca. 100 nm, given the high extinction coefficient for the material. This value is a constraint as far as the univocal determination of film thickness is concerned, without aid of secondary spectroscopic techniques. However, by changing the excitation wavelength to probe the films at non-resonant conditions, such maximum shifts to higher values (>200 nm depending on the excitation wavelength) and the Raman intensity curve starts oscillating throughout a broad thickness regime prior to saturation. Figures S-3(a)-(c) illustrate the changes in the interference curves obtained for the 1450 cm^{-1} mode in rr-P3HT under three different excitation wavelengths: (a) 488 nm, (b) 514 nm and (c) 633 nm. Whereas at 488 and 514 nm excitation resonant conditions are fulfilled, at 633 nm excitation the polymer is almost out-of-resonance as indicated by the low extinction coefficient. Consequently, if a certain rr-P3HT sample is measured using several excitation wavelengths exactly at the same locations we can perform a simultaneous fit of the Raman intensity at all wavelengths to overcome the oscillation of the intensity curves and to recover the uniqueness of the methodology. This approach is valid provided the intensity curves at all excitation wavelengths stay below their corresponding saturation regime, which location mainly depends on the magnitude of the extinction coefficient.

A similar approach can be applied in polymer:fullerene blends although the fullerene Raman cross-section is usually not high enough to identify its vibrational signature when it is excited out of resonance. Nevertheless, the signal due to the polymer will be damped by the presence of the fullerene in the scattering volume. This fact can be modelled as a lower *effective* thickness when measuring out of resonance and correlated with the volumetric fullerene fraction observed in resonance during the simultaneous fit.

In other cases the materials blended are incompatible in terms of the applicability of the methodology and alternative spectroscopic techniques must be selected instead to perform their characterization. P3HT:PCBM blends constitute an example in which neither the single-wavelength methodology nor the multi-wavelength fitting approach are successful. This is ascribed to the fact that the component Raman cross-sections are too dissimilar at all the excitation wavelengths used in this work (Table I in the manuscript) and their characteristic, most intense bands appear very close together (Fig. 1 in the manuscript). Such a difference hides the fullerene Raman signature in the measured spectra (at 488, 514 and 633 nm excitation) even in a 1:9 blend (w:w, P3HT:PCBM), hence rendering the fit inaccurate regarding film thickness and volumetric composition determination.

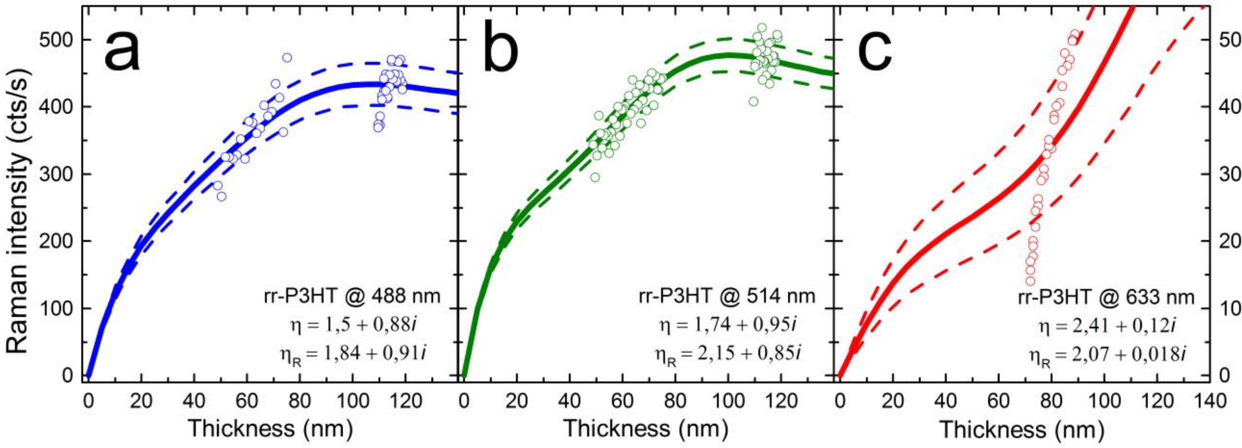

Figure S-3 Raman intensity of the 1450 cm^{-1} band in regio-regular P3HT as a function of film thickness for three excitation wavelengths: (a) 488 nm, (b) 514 nm and (c) 633 nm. The solid lines represent the best fit of the model to the experimental data with a single free parameter: the material's cross-section. The dashed lines stand for the standard deviation of the fit. The complex refractive indices attained at both the excitation wavelength (η) and the Raman-scattered light (η_R) are included at the bottom of each panel.

EVALUATION OF THE SENSITIVITY OF THE METHODOLOGY IN THIN-FILM ARCHITECTURES WITH HIGH REFRACTIVE INDEX CONTRAST

When there exists a high refractive index contrast between the Raman-active material deposited as thin film and the closest layers (usually the substrate), the electromagnetic field distribution promotes the Raman-scattered intensity to oscillate strongly at moderate film thickness values (50-300 nm). In this particular situation the accuracy in the determination of the optical constants for all layers in the multi-layered stack is critical to properly reproduce the experimental trends; in fact, Raman spectroscopy can be exploited to fine-tune the optical constants attained at a certain wavelength by fitting the Raman intensity oscillation as a function of film thickness.

As a significant example, we have explored the dependence of the 1353 cm^{-1} Raman band of C16-IDTBT deposited by blade coating as a graded film on a silicon substrate (with a native SiO_2 layer of ca. 5 nm). Figure S-4(a) illustrates the experimental trend obtained up to nearly 400 nm in thickness as well as the model prediction at 488 nm excitation. Clearly, the methodology cannot reproduce well the amplitude of the experimental intensity maxima although their position in terms of film thickness is the correct one. We have simultaneously studied the intensity of the silicon LO mode (520.7 cm^{-1}) as a function of polymer thickness and confirmed that the second Raman intensity maximum observed experimentally could not be successfully matched [Fig. S-4(b)].

We then proceeded to perform a fit of the experimental data using as free parameters the optical constants at 488 nm, at the silicon LO mode scattered wavelength (500.7 nm) and at the wavelength of the polymer 1353 cm^{-1} band (522 nm); see Figs. S-4(c)-S-4(d). In this case, the optical constants at 488 nm are shared in the modeling of silicon LO mode intensity and polymer band intensity. The fit results in an improved matching of the Raman intensity maxima and their location in terms of film thickness with respect to the experimental data. The optical constants obtained are experimentally acceptable given the uncertainty observed in C16-IDTBT films depending on the casting method used; see Fig. S-5. These results suggest that the accuracy of the material refractive index and extinction coefficient is critical when modeling the Raman intensity dependence in architectures with high refractive index contrast.

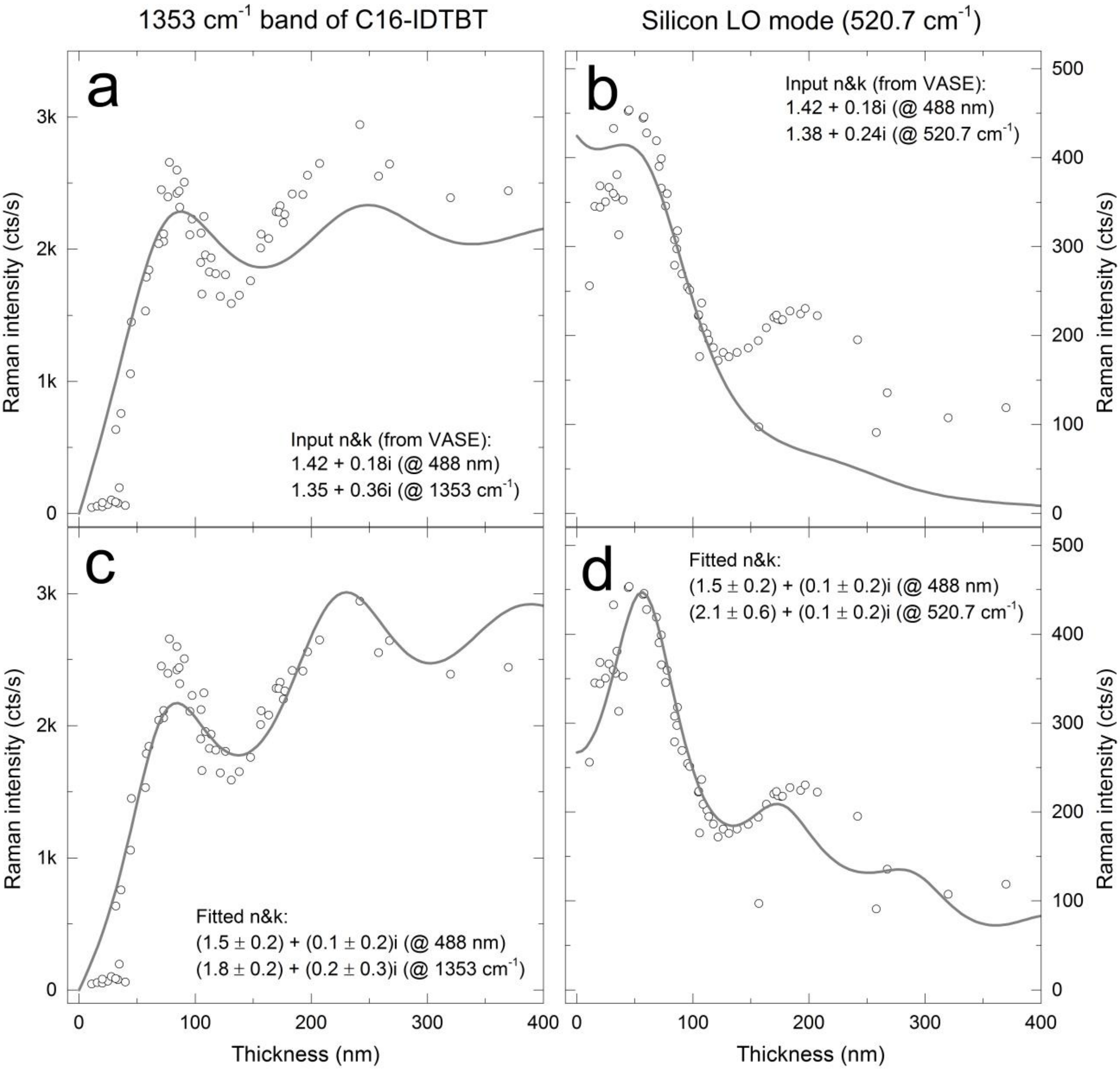

Figure S-4 Application of the methodology in a graded C16-IDTBT sample casted on a Si substrate (with a native oxide SiO_2 of ca. 5 nm, n = 1.46, k = 0). Solid lines represent the best fit to the experimental data (open circles). (a) Fit of the 1353 cm^{-1} mode intensity of C16-IDTBT using the optical constants extracted from VASE in a blade-coated, uniform sample; (b) fit of the Raman intensity of silicon LO mode (520.7 cm^{-1}) as a function of the polymer film thickness; (c) fit of the experimental data corresponding to the 1353 cm^{-1} polymer Raman mode using the optical constants as free parameters; (d) fit of the experimental data of the 520.7 cm^{-1} silicon LO mode using the optical constants as free parameters. Note that the complex refractive index at 488 nm is a shared parameter during the fit of (c) and (d) curves.

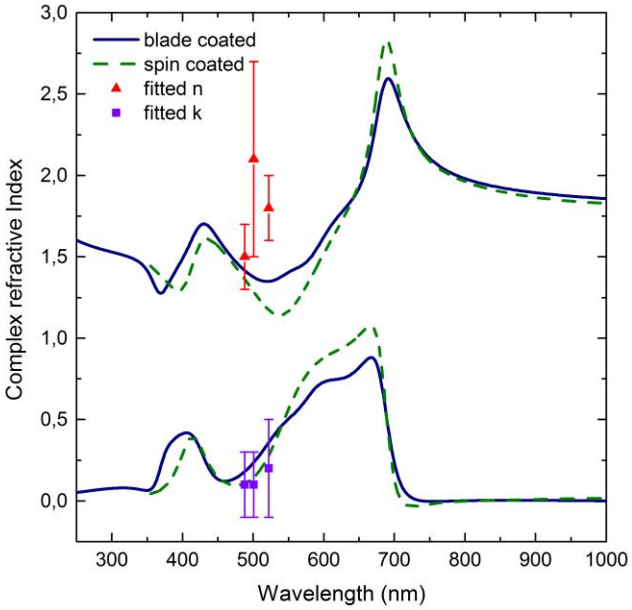

Figure S-5 Complex refractive index as obtained from VASE in C16-IDTBT samples prepared by two different methods on glass substrates: blade coating (blue solid line) and spin coating (green dashed line). The optical constants extracted from the fits in Figs. S-4(c)-S-4(d) are also included together with their corresponding error bars (standard deviations).

EFFECT OF PHOTODEGRADATION IN THE RAMAN SPECTRA OF SEVERAL CASE EXAMPLES

Conjugated materials are generally photodegraded upon exposure to a focused laser beam in an oxygen-rich atmosphere. The consequences of such degradation in terms of the vibrational Raman spectrum are mainly three: a large shift of the bands, an intensity variation and an increase of the photoluminescence background. A vast majority of the conjugated materials studied in this work follow a similar trend depending on the laser power arriving at the sample and the exposure time to the laser beam. Thus, the absence of photodegradation during the acquisition of the spectra is mandatory for the proper implementation, accuracy and reproducibility of the methodology. The rapid photobleaching in air of PCPDTBT:$PC_{70}BM$ films is demonstrated in Figs. S-6 and S-7, in which the evolution of the acquired spectra is illustrated as a function of the laser exposure time. In this particular type of blend, photodegradation increases both the overall Raman intensity due to the polymer as well as the background line, eventually hiding the Raman signature of $PC_{70}BM$ after 30 seconds of exposure. Thus the application of the methodology in these spectra results in an overestimation of the polymer content as the film is progressively degraded (see Fig. S-8), as well as a loss in accuracy in film thickness determination.

Photodegradation can be suppressed if the Raman experiments are performed either in vacuum (with a mechanical, rotatory pump) or in oxygen-free (inert) atmospheres. Even the blow of a nitrogen gun applied on the sample may be enough in some cases to slow down the photodegradation process (see Fig. S-8); this may be a valid option in the case of lack of suitable vacuum equipment or chambers, although it leads to poorer reproducibility than in vacuum. Apart from using inert atmospheres we have checked that if the Raman spectra are acquired in a time-scale below that in which significant photodegradation occurs, robust data can be obtained in ambient conditions. This is the case of our second setup (Alpha300RA by WITec), in which the integration time of the CCD camera can be reduced up to a few hundreds of milliseconds (30-500 ms). By exploiting this feature we can reduce the exposure time of the sample to the laser beam to harmless values in terms of photodegradation. This strategy may require an initial exploration step as the threshold exposure (and integration) time beyond which photodegradation arises. This time will depend on the power irradiance at the sample and the sensitivity of the material(s) analysed to the wavelength employed. In our setup (488 nm excitation with power values below 200 µW in free-beam conditions) we found that exposure times below 600 ms were enough to avoid the typical photodegradation signatures (peak shifting, intensity variations and increase of photoluminescence background) to disrupt the collected spectra, thus enabling the proper implementation of the methodology in air. This fact is illustrated in Fig. S-1(b) by the proper matching of the Raman intensity vs. film thickness dependence in a graded C16-IDTBT film. The data were acquired measuring on-the-fly at a constant lateral speed along the gradient direction. The integration times (and lateral speeds) were 536 ms (210 µm/s) and 336 ms (268 µm/s) for the 10X and 50X magnification objectives, respectively.

Nevertheless, there are conjugated materials in which photodegradation is not so critical, as it takes longer to manifest and to irreversibly disrupt the vibrational spectra. Neat fullerenes, as well as neat PCDTBT films and PCDTBT:$PC_{70}BM$ blends constitute examples of increased robustness in terms of photobleaching. Figure S-9 shows how such polymer:fullerene blends lead to a small difference in composition (below 5 vol%) when comparing the results obtained in air or in vacuum while using moderate integration times (5-10 seconds). However, such small mismatch in composition confirms that the exposure to the laser beam is affecting the integrity of the species in the film, although to a minor extent. Hence vacuum conditions are advised to achieve the maximum accuracy and reproducibility despite the apparent insensitivity of the materials to the laser exposure.

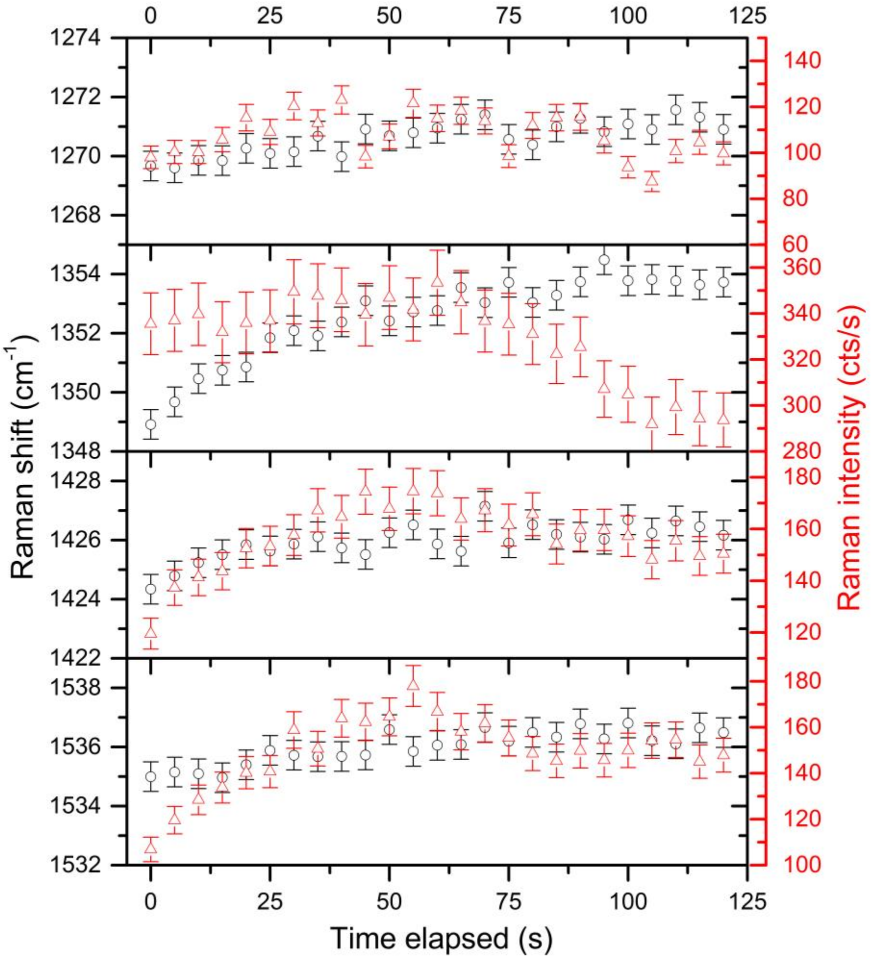

Figure S-6 Temporal evolution of the main Raman peak positions (black circles, left Y-axis) and intensities (red triangles, right Y-axis) in a pure PCPDTBT sample during exposure for two minutes to the laser beam (488 nm) in ambient conditions. Each data point corresponds to a single Raman spectrum acquired during 5 seconds of integration at the CCD. The zeroth step corresponds to the measurement performed in vacuum, which remains stable for hours.

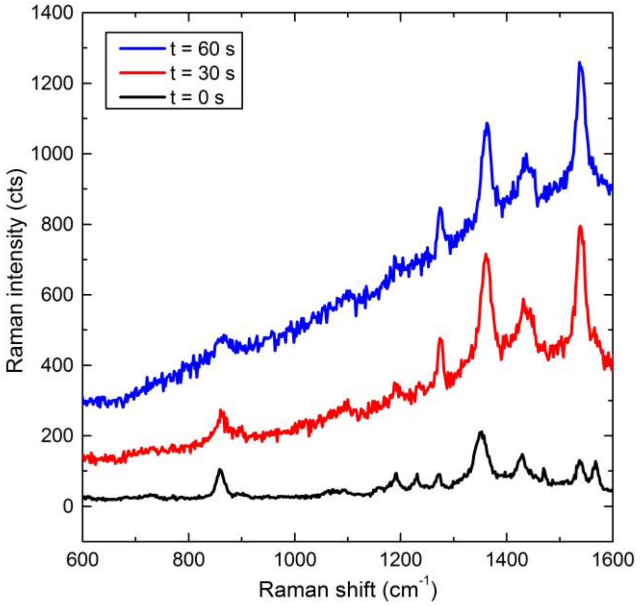

Figure S-7 Raman spectra due to a PCPDTBT:PC$_{70}$BM 1:1 (w:w) blend measured in air at 0 seconds (black), 30 seconds (red) and 60 seconds (blue) after laser exposure (488 nm). Note the increase on the photoluminescence background as the sample is exposed to the laser beam as well as the enhancement of the characteristic Raman modes due to the polymer, which eventually hide fullerene vibrational signature in the spectrum.

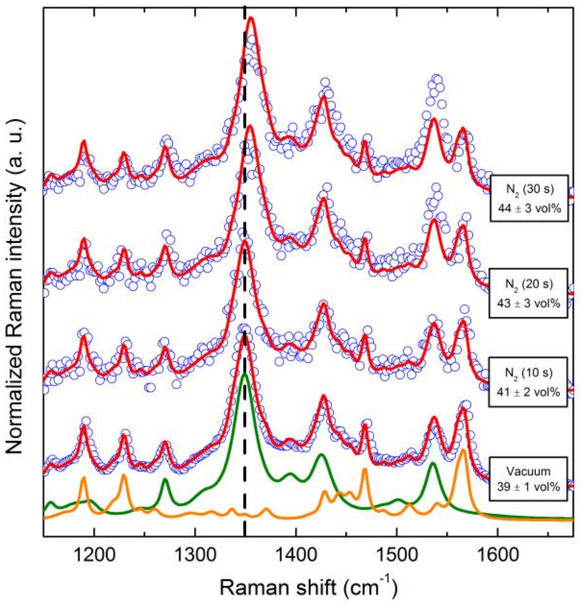

Figure S-8 Effect of photodegradation on the Raman spectrum of a 1:1 (w:w) PCPDTBT:PC$_{70}$BM blend as a function of the laser (488 nm) exposure time. Note how photodegradation is slowed down due to the blow of a nitrogen gun. The percentages refer to the polymer volume content as extracted from the fits. An extra degree of freedom is added to follow the position of the 1348 cm^{-1} band as the film is degraded. The red solid lines stand for the fit of the experimental data following the methodology described in the article, whereas the green and orange lines represent the Raman spectra due to PCPDTBT and PC$_{70}$BM, respectively.

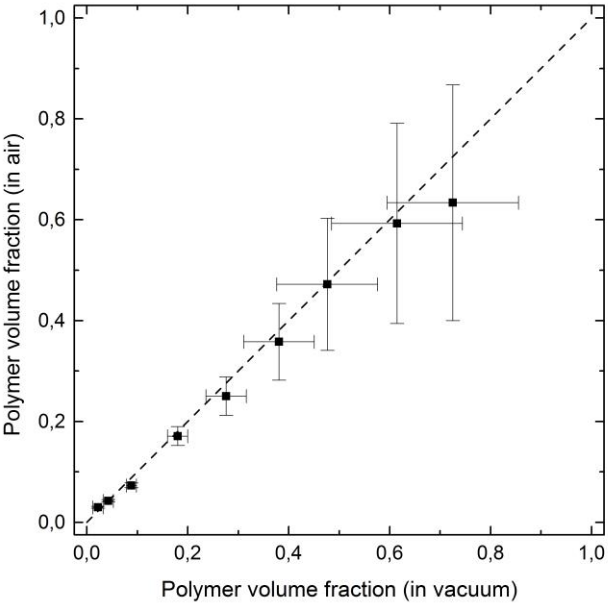

Figure S-9 The correlation between polymer volume fractions extracted in air and in vacuum with the use of Raman scattering at 488 nm excitation shows that PCDTBT:$PC_{70}BM$ blends are quite robust in terms of degradation.